Direct probing of the cluster structure in ^{12}Be via the α-knockout reaction

Mengjiao Lyu,[1,*] Kazuki Yoshida,[2,†] Yoshiko Kanada-En'yo,[3,‡] and Kazuyuki Ogata[1,4,5,§]

[1]*Research Center for Nuclear Physics (RCNP), Osaka University, Ibaraki 567-0047, Japan*
[2]*Advanced Science Research Center, Japan Atomic Energy Agency, Tokai, Ibaraki 319-1195, Japan*
[3]*Department of Physics, Kyoto University, Kyoto 606-8502, Japan*
[4]*Department of Physics, Osaka City University, Osaka 558-8585, Japan*
[5]*Nambu Yoichiro Institute of Theoretical and Experimental Physics (NITEP), Osaka City University, Osaka 558-8585, Japan*

(Received 8 February 2019; published 14 June 2019)

Background: Recent theoretical and experimental researches using proton-induced α-knockout reactions provide direct manifestation of α-cluster formation in nuclei. In recent and future experiments, α-knockout data are available for neutron-rich beryllium isotopes. In ^{12}Be, rich phenomena are induced by the formation of α clusters surrounded by neutrons; for instance, breaking of the neutron magic number $N = 8$.
Purpose: Our objective is to provide direct probing of the α-cluster formation in the ^{12}Be target through associating the structure information obtained by a microscopic theory with the experimental observables of α-knockout reactions.
Method: We formulate a new wave function of the Tohsaki–Horiuchi–Schuck–Röpke (THSR) type for the structure calculation of ^{12}Be nucleus and integrate it with the distorted-wave impulse-approximation framework for the α-knockout reaction calculation of ^{12}Be$(p, p\alpha)^{8}$He.
Results: We reproduce the low-lying spectrum of the ^{12}Be nucleus by using the THSR wave function and discuss the cluster structure of the ground state. Based on the microscopic wave function, the optical potentials and α-cluster wave function are determined and utilized in the calculation of ^{12}Be$(p, p\alpha)^{8}$He reaction at 250 MeV. The possibility of probing the clustering state of ^{12}Be through this reaction is demonstrated by analysis of the triple differential cross sections that depend sensitively on the α-cluster amplitude at the nuclear surface.
Conclusions: This study provides a feasible approach to validate directly the theoretical predictions of clustering features in the ^{12}Be nucleus through the α-knockout reaction.

DOI: 10.1103/PhysRevC.99.064610

I. INTRODUCTION

In atomic nuclei, the clusters emerge as a result of the competition between the short-range repulsion and the medium-range attraction induced by the Pauli blocking effect and the properties of nuclear forces [1]. In particular, the α-clustering effect is prevalent in nuclear clustering states because of the spin-isospin saturation in the nucleon-nucleon interaction. For the description of α-clustering states, various structural theories have been formulated, as introduced in Refs. [1–8] and references therein.

In the Hoyle state of ^{12}C, the α-cluster formation has been well established and the description of the clustering state has been treated elegantly in nuclear theory [9]. However, in neutron-rich nuclei, the description of the α-clustering states is more challenging because of the existence of valence neutrons surrounding α-clusters, as shown in the previous studies of Beryllium isotopes [10–25]. Especially, in ^{10}Be and ^{12}Be isotopes, the nuclear molecular orbit (MO) configuration and the ion-like binary cluster configuration could coexist in clustering states, as predicted by theoretical studies using the generalized two-center cluster model (GTCM) [20–22] and antisymmetrized molecular dynamics (AMD) [23–25]. In the ^{12}Be nucleus, the breaking of the neutron magic number $N = 8$ also occurs as a consequence of α-cluster formation [21–23].

In previous decades, the α-clustering states in stable nuclei have been investigated through the proton-induced α-knockout reactions [26–35]. The significant advantage in these studies is that the physical observables are directly connected to the α clusters [32,34,35], and the reaction mechanism is clean as compared with the other direct reactions where α clusters are involved, such as the α-transfer reactions [36–39]. The theoretical description of α-knockout reactions has been formulated by using the distorted-wave impulse-approximation (DWIA) framework [26,32,33,35] and, in recent works [32,35], the peripheral property of the $(p, p\alpha)$ reactions has been demonstrated. This is essential for probing α clusters, which are most probably formed in the surface region of nuclei. Recently, there are emerging $(p, p\alpha)$

*mengjiao@rcnp.osaka-u.ac.jp
†yoshidak@rcnp.osaka-u.ac.jp
‡yenyo@ruby.scphys.kyoto-u.ac.jp
§kazuyuki@rcnp.osaka-u.ac.jp

reactions in inverse kinematics for light unstable nuclei including the neutron-rich Be isotopes that is conducted or planned in the Radioactive Isotope Beam Factory (RIBF) [40]. These experiments provide ideal opportunities to investigate the clustering states of the neutron-rich Be isotopes by comparing theoretical predictions of $(p, p\alpha)$ reaction observables and the corresponding experimental results.

In our previous work, we investigated the ^{10}Be$(p, p\alpha)^{6}$He reaction at 250 MeV by integrating the microscopic description of the ^{10}Be target and the ^{6}He residual nuclei into the DWIA framework for the α-knockout reaction and predicted the triple-differential cross sections (TDX) as a useful observable probing the α clustering in the ^{10}Be nucleus [34]. For the structure calculation of the ground state of ^{10}Be and ^{6}He, Tohsaki–Horiuchi–Schuck–Röpke (THSR) wave functions have been formulated based on previous studies [9,41–49].

In this work, we further extend the THSR wave function for the ^{12}Be nucleus. The theoretical description of the clustering features of the ^{12}Be nucleus is not so simple as those of the ^{10}Be nucleus because of the coexistence of binary cluster and MO configurations. It is essential to take into account these different cluster configurations for the description of the ground state of ^{12}Be nucleus; in particular, the phenomena of the $N = 8$ magic number breaking. In this study, we show that the TDX can be the direct probe for such exotic clustering features in the ^{12}Be nucleus. In addition, this work provides a new formulation of the THSR wave function for the neutron-rich nucleus ^{12}Be, which could be utilized in further studies of other nuclei near the neutron drip line.

This article is organized as follows: In Sec. II, we recapitulate the DWIA framework for the α-knockout reaction and the calculation of triple-differential cross sections (TDX). In Sec. III, we formulate the THSR wave functions for the ^{12}Be target and the ^{8}He residual, and the extraction of the α-cluster wave function. Some details of the formulation are given in the Appendix. In Sec. IV, we discuss the numerical results for the nuclear structure of ^{12}Be and the predictions of ^{12}Be$(p, p\alpha)^{8}$He reaction observables (TDXs). Section V contains the conclusion.

II. DISTORTED-WAVE IMPULSE-APPROXIMATION FRAMEWORK FOR ^{12}Be$(p, p\alpha)^{8}$He REACTION

We adopt the same DWIA framework as in Refs. [32,35] for the $(p, p\alpha)$ reaction. In this section, we introduce briefly the DWIA framework for the ^{12}Be$(p, p\alpha)^{8}$He reaction. The coordinates for the description of the α-knockout reaction are presented in Fig. 1. Here, the normal kinematics is adopted for simplicity. The transition amplitude for the $(p, p\alpha)$ reaction is given by

$$T_{\boldsymbol{K}_0\boldsymbol{K}_1\boldsymbol{K}_2} = \left\langle \chi^{(-)}_{1,\boldsymbol{K}_1}(\boldsymbol{R}_1)\chi^{(-)}_{2,\boldsymbol{K}_2}(\boldsymbol{R}_2)\middle| t_{p\alpha}(\boldsymbol{s})\middle|\chi^{(+)}_{0,\boldsymbol{K}_0}(\boldsymbol{R}_0)\varphi_\alpha(\boldsymbol{R}_2)\right\rangle, \quad (1)$$

where the χ with subscripts 0, 1, and 2 denote the distorted wave functions for the incident proton p, the outgoing p, and the outgoing α, respectively. The superscripts $(+)$ and $(-)$ indicate the outgoing and incoming boundary conditions adopted for χ, respectively. The φ_α is the α-cluster wave function inside the target nucleus ^{12}Be, where only the 0^+ channel is included. For each particle $i = 0, 1, 2$, the momentum (wave number) and its solid angle in the center-of-mass frame are denoted by $\boldsymbol{K}_i$ and Ω_i, respectively, and the corresponding quantities measured in the laboratory frame are denoted by additional superscript L. We follow the theoretical approach in Ref. [32] for the numerical calculation of the triple differential cross section (TDX) of the ^{12}Be$(p, p\alpha)^{8}$He reaction:

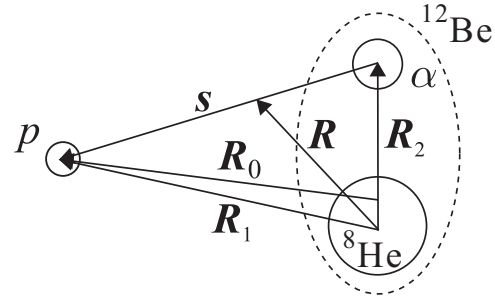

FIG. 1. Coordinates of the ^{12}Be$(p, p\alpha)^{8}$He reaction.

$$\frac{d^3\sigma}{dE_1^{\mathrm{L}}d\Omega_1^{\mathrm{L}}d\Omega_2^{\mathrm{L}}} = F_{\mathrm{kin}}C_0\frac{d\sigma_{p\alpha}}{d\Omega_{p\alpha}}\left|\bar{T}_{\boldsymbol{K}_0\boldsymbol{K}_1\boldsymbol{K}_2}\right|^2, \quad (2)$$

$$\bar{T}_{\boldsymbol{K}_0\boldsymbol{K}_1\boldsymbol{K}_2} = \int d\boldsymbol{R}\,\chi^{(-)}_{1,\boldsymbol{K}_1}(\boldsymbol{R})\chi^{(-)}_{2,\boldsymbol{K}_2}(\boldsymbol{R})\chi^{(+)}_{0,\boldsymbol{K}_0}(\boldsymbol{R})\varphi_\alpha \times (\boldsymbol{R})e^{-i\boldsymbol{K}_0\cdot\boldsymbol{R}A_\alpha/A}, \quad (3)$$

where $A_\alpha = 4$ and $A = 12$. F_{kin} and C_0 are kinematical factors, and $d\sigma_{p\alpha}/d\Omega_{p\alpha}$ is the p-α differential cross section at the energy and the scattering angle deduced from the $(p, p\alpha)$ kinematics. $\bar{T}_{\boldsymbol{K}_0\boldsymbol{K}_1\boldsymbol{K}_2}$ is a reduced transition amplitude obtained by making the factorization approximation to Eq. (1); details can be found in Ref. [32].

In this calculation, the optical potentials for the p-^{12}Be, p-^{8}He, and α-^{8}He systems and the transition interaction $t_{p\alpha}$ between p and α are determined by the folding model using the Melbourne G-matrix interaction [50]. The density distributions of the target and residual nuclei are extracted from the THSR wave function, which is formulated in Sec. III, and the phenomenological density distribution is adopted for the α cluster as introduced in Ref. [32]. The spin-orbit part of each optical potential was disregarded. The distorted wave functions χ_i $(i = 1, 2, 3)$ are obtained by solving the corresponding Schrödinger equations by using the optical potentials mentioned above. The α-cluster wave function φ_α is extracted from the THSR wave function of ^{12}Be by approximating the reduced width amplitude (RWA), as introduced in Sec. III C.

III. TOHSAKI–HORIUCHI–SCHUCK–RÖPKE WAVE FUNCTION FOR TARGET AND RESIDUAL NUCLEI

We formulate the THSR wave functions for the target and residual nuclei by extending the microscopic models developed in previous works [47–49]. For the target nucleus ^{12}Be, we consider three kinds of cluster configurations suggested in the theoretical works [21,23] as basis states in the THSR framework of nonlocalized cluster motion [44,45]. One is the

binary cluster configuration

$$\alpha + {}^{8}\mathrm{He}, \tag{4}$$

and the other two are the MO configurations

$$\begin{aligned} \pi\text{-orbit:} \quad & 2\alpha + 2n(\pi) + 2n(\pi*), \\ \sigma\text{-orbit:} \quad & 2\alpha + 2n(\pi) + 2n(\sigma). \end{aligned} \tag{5}$$

It has been suggested in Ref. [21] that the binary cluster configuration $\alpha + {}^{8}$He dominates in ^{12}Be when the two α clusters are well separated, while the MO configurations contribute when the α-α distance is less than 6 fm. In what follows, we refer these three configurations as "$\alpha + {}^{8}$He," "π orbit," and "σ orbit," respectively.

A. $\alpha + {}^{8}$He configuration of ^{12}Be

In this work, we describe the $\alpha + {}^{8}$He configuration of ^{12}Be in the THSR framework as

$$|\Phi_{\alpha+{}^{8}\mathrm{He}}\rangle = \int d\boldsymbol{R}\, \mathcal{G}(\boldsymbol{R}, \boldsymbol{\beta}_\alpha) |\mathcal{A}\{\Phi_\alpha(-\boldsymbol{R})\Phi({}^{8}\mathrm{He}, \boldsymbol{R})\}\rangle, \tag{6}$$

where the formulation of the ^{8}He cluster wave function $\Phi({}^{8}\mathrm{He}, \boldsymbol{R})$ is explained in the Appendix. Similar formulation for the $\alpha + {}^{16}$O configuration has been proved to be very efficient in describing the ground state of ^{20}Ne in Refs. [44,45]. We note that, in the THSR framework, each basis wave function expresses not localized α and ^{8}He clusters but nonlocalized clusters with almost free motion, which is different from the basis states used in other models [18,21].

B. Molecular orbit configurations of ^{12}Be

The π-orbit configuration of ^{12}Be is written as

$$\begin{aligned} |\Phi_{\pi\text{-orbit}}\rangle = \int d\boldsymbol{R} \mathcal{G}(\boldsymbol{R}, \boldsymbol{\beta}_\alpha) \big| \mathcal{A}\big\{ & \Phi_\alpha(-\boldsymbol{R}) \\ & \times \Phi_\alpha(\boldsymbol{R}) \phi^{\pi}_{10} \phi^{\pi}_{10} \phi^{\pi*}_{11} \phi^{\pi*}_{12} \big\} \big\rangle, \end{aligned} \tag{7}$$

where the function $\mathcal{G}$ is the deformed Gaussian for describing the nonlocalized motion of two α clusters within the ^{12}Be nucleus, which is defined by

$$\mathcal{G}(\boldsymbol{R}, \boldsymbol{\beta}) = \exp\left(-\frac{R_x^2 + R_y^2}{\beta_{xy}^2} - \frac{R_z^2}{\beta_z^2} \right). \tag{8}$$

The four valance neutrons occupying the π orbits are described by the $\phi^{\pi}_{9,10}$ and $\phi^{\pi*}_{11,12}$ states, which correspond to the parallel and antiparallel spin-orbit couplings, respectively. The formulation of single nucleon states ϕ_9–ϕ_{12} are explained in the Appendix. In Fig. 2(a), the density distribution is presented for ϕ_{11} and ϕ_{12}, in which the typical structure of the π-orbit configuration is clearly demonstrated. This π-orbit configuration goes to the p-shell closed configuration in the compact limit of the α cluster and valence neutron motions.

The σ-orbit configuration of ^{12}Be is formulated as

$$|\Phi_{\sigma\text{-orbit}}\rangle = \int d\boldsymbol{R}\, \mathcal{G}(\boldsymbol{R}, \boldsymbol{\beta}_\alpha) \big| \mathcal{A}\big\{ \Phi_\alpha(-\boldsymbol{R}) \Phi_\alpha(\boldsymbol{R}) \phi^{\pi}_{9} \phi^{\pi}_{10} \phi^{\sigma}_{11} \phi^{\sigma}_{12} \big\} \big\rangle, \tag{9}$$

where ϕ^{π}_{9} and ϕ^{π}_{10} are the same π states as in Eq. (7) and ϕ^{σ}_{11} and ϕ^{σ}_{12} are states for valance neutrons occupying the σ orbits. The formulation of ϕ_{11} and ϕ_{12} are explained in the Appendix. We also show the density distributions of ϕ^{σ}_{11} and ϕ^{σ}_{12} in Fig. 2(b), where the typical nodal structure in the σ orbit is reproduced. As seen in Fig. 2(c), the $\alpha + {}^{8}$He configuration also has a similar nodal structure of the valence neutrons along the $x = 0$ axis as a result of the antisymmetrization effect between neutrons in the α and ^{8}He clusters. In fact, the σ-orbit configuration is redundant in the present framework because it is already included in model space when the THSR bases of the $\alpha + {}^{8}$He configuration are superposed, as discussed in the Sec. IV B.

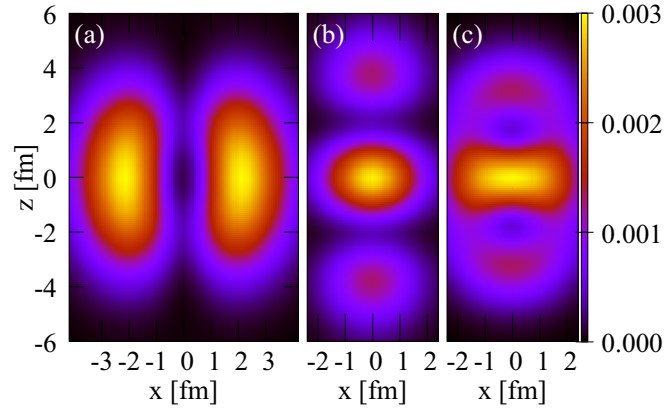

FIG. 2. Panels (a) and (b) show the distributions of valance neutrons of ^{12}Be occupying π and σ molecular orbits, respectively, as defined in Eqs. (A9) and (A13). The panel (c) shows the density distribution of valance neutron occupying the vertical p-orbit states of the ^{8}He cluster in the $\alpha + {}^{8}$He configuration of ^{12}Be, as defined in Eqs. (6) and (A7). Parameters for each configuration are listed in Table II in the Appendix.

C. Total wave function and α-cluster wave function of target nucleus

The total wave function of ^{12}Be is obtained by superposing the basis states in the three configurations formulated in Eqs. (6), (7), and (9). For each configuration, we formulate basis wave functions with different $\beta_{\alpha,z}$ parameters that manipulate the motion of clusters, and set other parameters to be the variationally optimized values for each configuration. All the parameters in the THSR bases are listed in Table II in the Appendix. The translational and rotational projections are performed for the bases to restore corresponding symmetry, as introduced in Ref. [47]. With these bases, the total wave function of ^{12}Be can be written as

$$|\Psi^{J}({}^{12}\mathrm{Be})\rangle = \sum_{m,j} c_{m,j} \hat{P}^{J}_{00} \hat{P}_{\mathrm{c.o.m}} \Phi_m(\beta_{\alpha,z;j}), \tag{10}$$

where Φ_m labeled by m for cluster configurations are the THSR bases for ^{12}Be and j denotes the choice of the parameter $\beta_{\alpha,z}$. The operators $\hat{P}^{0}_{00}$ and $\hat{P}_{\mathrm{c.o.m}}$ denote angular-momentum projection [51] and the projection for center-of-mass motion [10], respectively. The $c_{i,j}$ are superposition coefficients to be obtained by diagonalizing the Hamiltonian matrix.

To extract the α-cluster amplitude in the surface region, we approximate RWA $y(a)$ of the α cluster by the overlap of the total wave function of ^{12}Be in Eq. (10) with the $\alpha + {}^8$He cluster wave function as

$$|ay(a)| \approx ay^{\rm app}(a) \equiv N_c \left|\left\langle \Phi(^{12}\mathrm{Be}) \middle| \Phi^{(0+)}_{\rm BB}(^8\mathrm{He}, \alpha, S = a)\right\rangle\right|, \quad (11)$$

where

$$N_c = \frac{1}{\sqrt{2}}\left(\frac{8\times 4}{12\pi b^2}\right)^{1/4}, \quad (12)$$

with $\Phi_{\rm BB}(^8\mathrm{He}, \alpha, S)$ being a Brink–Bloch-type wave function [52] for the $\alpha + {}^8$He two-body system separated with the relative distance S:

$$\left|\Phi^{(0+)}_{\rm BB}(^8\mathrm{He}, \alpha, S)\right\rangle = \hat{P}^0_{00}\left|\phi\left(\alpha, \tfrac{8}{12}S\vec{e}_z\right)\Phi\left(^8\mathrm{He}(0^+), -\tfrac{4}{12}S\vec{e}_z\right)\right\rangle. \quad (13)$$

Here $\Phi(^8\mathrm{He}(0^+), -\frac{4}{12}S\vec{e}_z)$ is the wave function of the residual nucleus ^{8}He projected onto the 0^+ state, which is located at $-(4/12)S\vec{e}_z$. The $y^{\rm app}(a)$ is found to be a good approximation of the exact $y(a)$ in the surface region [53] and applicable to the present case because the observables in knockout reactions are only affected by the α-cluster probability at the surface [34].

IV. RESULTS

A. Numerical inputs

In this study, we fix the following kinematical conditions for the ^{12}Be$(p, p\alpha)^8$He reaction in the laboratory frame. The kinetic energy for the incident and emitted protons are set to be 250 and 180 MeV, respectively. The emission angle of the outgoing proton is set to be $(\theta^{\rm L}_1, \phi^{\rm L}_1) = (60^\circ, 0^\circ)$. To satisfy the recoilless condition for the ^{8}He residue, the angle $\theta^{\rm L}_2$ of the emitted α cluster varies around 51°, and the angle $\phi^{\rm L}_2$ is set as 180°. The relativistic treatment is adopted in all the reaction kinematics in this calculation as well as the kinematics of the p-α binary collision. Recently, the importance of the dynamical relativistic corrections to the Coulomb and nuclear interactions has been revealed for the breakup reactions [54–57]. To see the effect of the dynamical relativistic corrections in the $(p, p\alpha)$ knockout reactions will be interesting, but it is beyond the scope of current study.

For the Hamiltonian of ^{12}Be in the structural calculation, we adopt the MV1 interaction [58] of the central force, which includes finite-range two-body term and zero-range three-body terms. The two-body spin-orbit term is adopted from the G3RS interaction [59]. The parameters in these interactions and the width b of the Gaussian wave packet adopted here are those used in Ref. [23], where the energy spectra of low-lying states in ^{11}Be and ^{12}Be nuclei are well reproduced by the AMD calculations [23,60].

B. Energy spectrum of ^{12}Be nucleus

We calculate the energy and the wave function of ^{12}Be by diagonalizing the Hamiltonian with respect to the basis states formulated in Sec. III. First, we discuss the properties of the bases in each cluster configuration; that is, π orbit, σ orbit, or $\alpha + {}^8$He. In Fig. 3, the energies are plotted as functions of the parameter $\beta_{\alpha,z}$, which specifies the spatial extent of cluster motion. One sees clear dependence of the energy on $\beta_{\alpha,z}$ for all the three configurations. In the π-orbit (dashed curve) configuration, the energy minimum locates at about 2 fm, which corresponds to a very compact α-clustering structure due to the external bounding from valance neutrons in π states. In the σ-orbit (solid curve) and $\alpha + {}^8$He (dotted curve) configurations, the energy minima locate at much larger $\beta_{\alpha,z} = 4$ fm, which corresponds to very large spatial distribution of α clusters. In addition, the energies described by the π-orbit and $\alpha + {}^8$He configurations are found to be comparable with each other, which indicates that the breaking of the neutron magic number $N = 8$ could occur through a strong state mixing between these two configurations in the ground state of ^{12}Be. The bases in the σ-orbit configuration are energetically unfavored compared with the other two configurations and could give small contribution to the ground state of ^{12}Be.

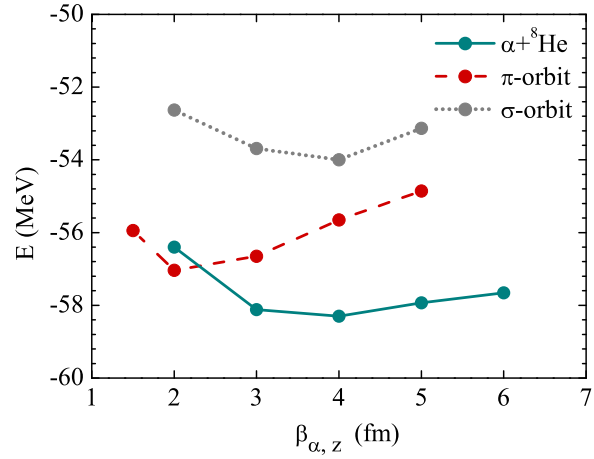

FIG. 3. Energy curves versus the variation of parameter $\beta_{\alpha,z}$ in the π-orbit (dashed), σ-orbit (dotted), and $\alpha + {}^8$He (solid) configurations of ^{12}Be.

In numerical calculations, we prepare the THSR bases with various parameters $\beta_{\alpha,z}$ in the π-orbit, σ-orbit and $\alpha + {}^8$He configurations. After the diagonalization of the Hamiltonian matrix, it is found that the total wave function of the ground state of ^{12}Be is efficiently described only by bases of the π-orbit and $\alpha + {}^8$He configurations. However, the σ-orbit configuration gives negligible contribution because the σ-orbit bases have large overlap with the corresponding $\alpha + {}^8$He bases and its contribution to the ground state can be effectively taken into account by the $\alpha + {}^8$He configuration in the THSR framework. Therefore, for the final result of ^{12}Be, we omit the σ-orbit bases and adopt six bases of the $\alpha + {}^8$He and π-orbit configurations by choosing $\beta_{\alpha,z} = 2, 3, 4$ fm for each configuration in the superposition given by Eq. (10).

The calculated energy spectrum for low-lying states 0^+_1, 0^+_2, and 2^+_1 of ^{12}Be are listed in Table I. For the ground state, we obtain the binding energy of −59.5 MeV, which is

TABLE I. The energy (E in MeV) of the ground state and excitation energies (ΔE in MeV) of the 0_2^+ and 2_1^+ states in ^{12}Be calculated with the superposition of the six bases from π-orbit and $\alpha + {}^8$He configurations. The MV1 potential and G3RS potential are used for interactions in the central and spin-orbit channels, respectively. Parameters of these potentials are adopted from Ref. [23]. "THSR" denotes the results calculated in this study using the THSR wave function. "AMD" denotes the results from the AMD investigations using the same interaction as in Ref. [23]. "THSR (weakened V_0^{ls})" denotes the results calculated using the same THSR bases as in Eq. (10) but with weakened spin-orbit coupling strength $V_0^{ls} = 3000$ MeV. "Expt." denotes corresponding experimental values.

^{12}Be	$E(0_1^+)$	$\Delta E(0_2^+)$	$\Delta E(2_1^+)$
THSR	−59.5	4.1	2.2
AMD	−61.9	3.7	2.1
Expt.	−68.6	2.3	2.1
THSR (weakened V_0^{ls})	−58.0	4.6	3.0

somewhat higher than the experimental value but acceptable because our main purpose is to describe correctly the cluster wave functions and to reproduce the energy spectrum, not to precisely reproduce the total energy. In particular, the excitation energy of the 2_1^+ state is very sensitive to the moment of inertia determined by the distribution of the α clusters. In this work, we reproduce well the energy gap for the ground band as $\Delta E(2_1^+) = 2.2$ MeV, which is consistent with the experimental value 2.1 MeV. As a comparison, we also show the results calculated by using the same THSR bases as in Eq. (10) but with a weakened spin-orbit coupling strength $V_0^{ls} = 3000$ MeV (the default value is 3700 MeV in Ref. [23]). The calculation with the weakened spin-orbit strength shows the higher excitation energy of $\Delta E(2_1^+) = 3.0$ MeV than the experimental value and may indicate a weaker α clustering in the ground band. The excitation energy calculated for the 0_2^+ state is 4.1 MeV with the default parameter in this study, which is consistent with the corresponding AMD result of 3.7 MeV but still higher than the experimental value.

C. Mixture of configurations in the ^{12}Be nucleus

The mixture of the π-orbit and $\alpha + {}^8$He configurations is explicitly treated as shown in Eq. (10). To discuss the contribution from the cluster configurations to the total wave function of ^{12}Be, we define a probability to find each configuration in the total wave function by

$$P_m = \frac{|\langle \Psi(^{12}\mathrm{Be})|\Phi'_m\rangle|^2}{\langle \Psi(^{12}\mathrm{Be})|\Psi(^{12}\mathrm{Be})\rangle \langle \Phi'_m|\Phi'_m\rangle}, \tag{14}$$

where $\Psi(^{12}\mathrm{Be})$ is the total wave function of ^{12}Be in Eq. (10) and Φ' is defined by

$$\Phi'_m = \sum_{j=1,2,3} c_{m,j} \hat{P}^0_{00} \hat{P}_{\mathrm{c.o.m}} \Phi_m(\beta_{\alpha,z;j}), \tag{15}$$

with $\beta_{\alpha,z;\{j=1,2,3\}} = \{2, 3, 4$ fm$\}$ and where the label m denotes π orbit or $\alpha + {}^8$He within the two configurations. Here the coefficients c_i are fixed to be the values determined by the full diagonalization for six bases.

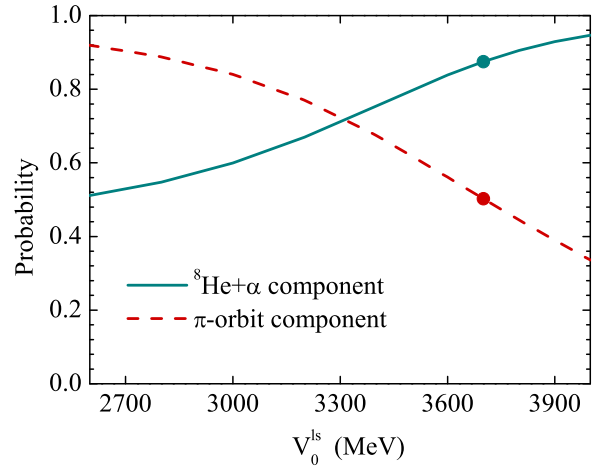

FIG. 4. The probability to find the $\alpha + {}^8$He (solid curve) and π-orbit (dashed curve) components in the total wave function for the ground state of ^{12}Be. The horizontal axis is the spin-orbit coupling strength V_0^{ls}. The solid dots are the values that correspond to the default choice of V_0^{ls}.

In Fig. 4, we show the probability of each component in the total wave function of ^{12}Be. The probabilities of the π-orbit (dashed curve) and $\alpha + {}^8$He (solid curve) components are plotted as functions of the spin-orbit coupling strength V_0^{ls}. A strong dependence on V_0^{ls} is observed for the mixing ratio between the two configurations. As the spin-orbit coupling strength increases, the $\alpha + {}^8$He component increases because the $\alpha + {}^8$He configuration comes to the energy relatively lower than the π-orbit configuration as shown in Fig. 3. As a consequence, the dominant component is changed from the π-orbit to the $\alpha + {}^8$He configuration, which simulates the gradual transition from the normal state to the intruder state in the ground-state wave function. With the default choice of $V_0^{ls} =$ 3700 MeV, the ground state of ^{12}Be contains a 90% $\alpha + {}^8$He component and have a largely developed α clustering. With a weakened spin-orbit coupling strength $V_0^{ls} = 3000$ MeV, the $\alpha + {}^8$He component reduces significantly to about 60% corresponding to the modest α clustering. It should be noted that the π-orbit and $\alpha + {}^8$He configurations are not orthogonal to each other and the ground state also has 50% and 80% π-orbit probabilities for the default and weakened V_0^{ls} cases, respectively. Considering that the V_0^{ls} and other parameters in the NN interactions are model dependent in different microscopic calculations, the ambiguities are inevitable for the mixing ratios between clustering configurations. Hence, the experimental observables that are directly related to these mixing ratios are essential for the validation of the predictions from the nuclear theories.

D. The α-cluster wave function

The α-cluster wave function of ^{12}Be can be obtained with the approximated RWA as described in Sec. III C. In Fig. 5, we compare the approximated RWAs for the THSR bases in the $\alpha + {}^8$He (solid curve), π-orbit (dashed curve), and σ-orbit

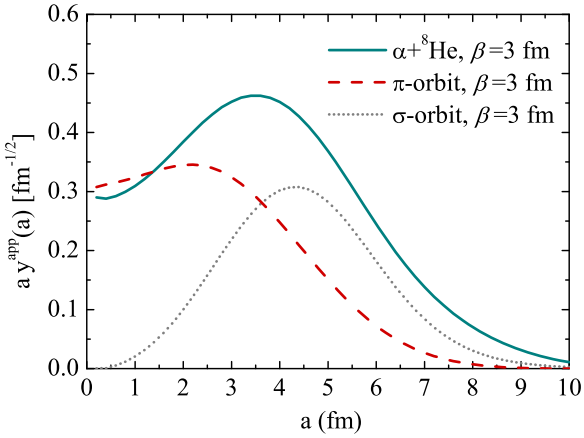

FIG. 5. Comparison of approximated RWAs for the THSR bases in the $\alpha + {}^{8}$He (solid curve), π-orbit (dashed curve), and σ-orbit (dotted curve) configurations of ^{12}Be. Formulations of each basis are introduced in the text and the parameter $\beta_{\alpha,z}$ is set to 3 fm.

(dotted curve) configurations. It is clearly shown that the $\alpha + {}^{8}$He configuration shows a much larger amplitude at the surface region because it describes the enhanced α clustering compared with in the π-orbit configurations. We note again that the cross sections of the α-knockout reaction are sensitive to the α amplitudes in the surface region but are not affected by the amplitudes in the inner region.

In Fig. 6, we compare the approximated RWAs for the ^{12}Be target with the default interaction (solid curve) and that with the weakened spin-orbit coupling strength (dashed curve). In the surface region, a significant difference is observed for the α amplitudes between the curves. The calculation with the default interaction gives larger surface amplitude than with the weakened spin-orbit coupling strength because of the larger $\alpha + {}^{8}$He component. As shown in Sec. IV E, this difference in the α amplitudes in the surface region can be examined by the TDX observables in the α-knockout reaction.

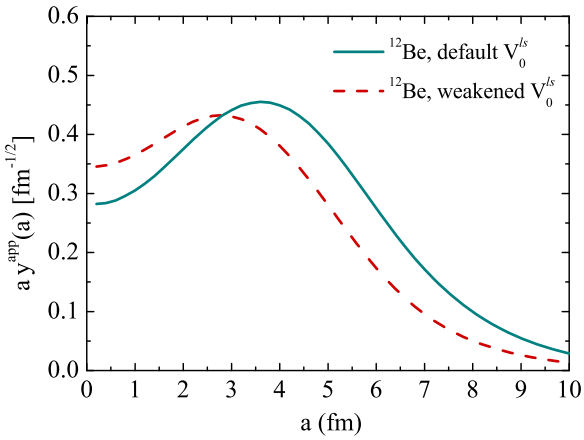

FIG. 6. The approximated RWAs for the ^{12}Be target with the default interaction (solid curve) and the weakened spin-orbit coupling strength (dashed curve).

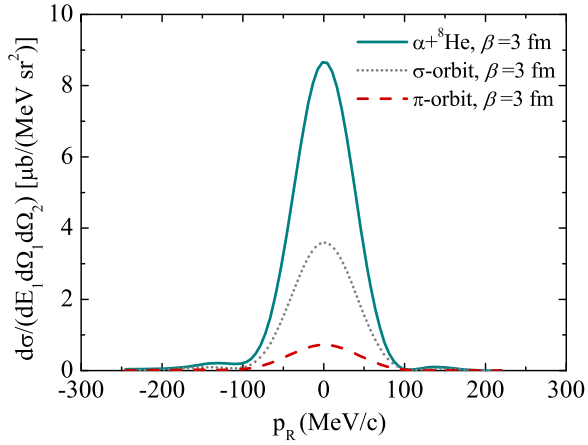

FIG. 7. Comparison of TDXs calculated by using one THSR basis in each of the $\alpha + {}^{8}$He, σ-orbit, and π-orbit configurations. Parameters $\beta_{\alpha,z}$ in these bases are set to 3 fm. The same kinematics is adopted as in Fig. 8.

E. Triple-differential cross sections

In Fig. 7, the TDXs are compared for the THSR bases in the $\alpha + {}^{8}$He (solid curve), σ-orbit (dotted curve), and π-orbit (dashed curve) configurations with $\beta_{\alpha,z} = 3$ fm. A prominent TDX is obtained for the solid curve, which is a logical outcome of the strong α clustering in the $\alpha + {}^{8}$He configuration. On the other hand, the dashed curve has a significantly lower peak height, which is consistent to the weak α clustering in the π-orbit configuration. The huge difference in the magnitude with a factor of 10 between these two configurations indicates that the $(p, p\alpha)$ reactions could be used as a sensitive tool to differentiate the mixing of the strong- and weak-clustering components. For the σ-orbit configuration, we note that the dashed curve in Fig. 7 shows the TDX with about half the magnitude of the solid curve, as expected from the RWA shown in Fig. 5, where a ratio of about 0.5 is obtained for the squared values between the σ-orbit and the $\alpha + {}^{8}$He configurations.

In Fig. 8, the theoretical predictions of the TDXs are shown. When the default V_0^{ls} is adopted in the NN interaction, as shown by the solid curve in Fig. 8, the TDXs are found to be analogous to the values of the $\alpha + {}^{8}$He configuration in Fig. 7. In this case, the neutron magic number $N = 8$ apparently breaks because of the intruder occupation induced by the α-cluster formation. The dashed curve in Fig. 8 corresponds to the weakened $V_0^{ls} = 3000$ MeV, where the intermediate strength of α-cluster formation is suggested by the probability calculation in Fig. 4, and we expect weaker breaking of $N = 8$ than in the default case. The ratio of about two is observed for the TDXs between the default and weakened curves at zero momentum. We stress again that the TDX curves are sensitive to α clustering in the wave function. In particular, this difference is much larger than in the RWA curves in Fig. 6.

In both Figs. 7 and 8, the high sensitivities of the $(p, p\alpha)$ reaction are established for clarifying the strong and the weak α-clustering. We credit this superiority to the peripheral property of the $(p, p\alpha)$ reaction [32,35], which allows probing of the α clusters only in the surface region where the probability

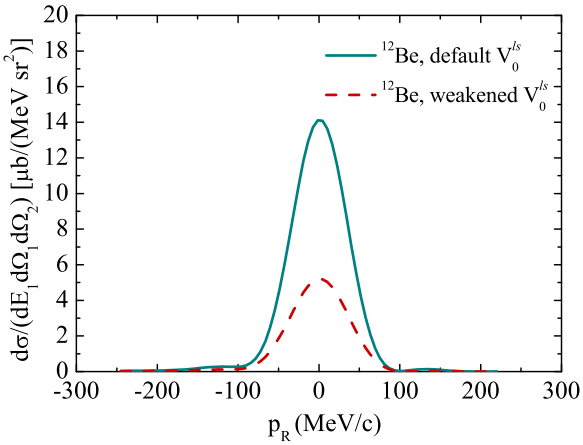

FIG. 8. The TDXs of the ^{12}Be$(p, p\alpha)^8$He reaction at 250 MeV, predicted by calculations using the default and the weakened spin-orbit coupling strength. Kinetic energy of particle 1 is fixed at 180 MeV and its emission angle is set to $(\theta_1^{\rm L}, \phi_1^{\rm L}) = (60^\circ, 0^\circ)$. $\phi_2^{\rm L}$ is fixed at 180° and $\theta_2^{\rm L}$ is varied around 51°. P_R is the recoil momentum.

of cluster formation is the largest. Hence, by comparing the experimental values of TDX with the theoretical predictions in Figs. 7 and 8, we can validate the breaking of $N = 8$ by cluster formation. Furthermore, differentiation between the strong and the weak α clustering in the ground state of ^{12}Be will be feasible.

Recently, there have been several works regarding the use of eikonal scattering waves in the DWIA framework for the $(p, 2p)$ reactions [61–63]. It will be interesting to evaluate the efficiency of eikonal approximation in the current $(p, p\alpha)$ case, which is expected to be discussed in our future work.

V. SUMMARY

We have provided the direct probing for the α-clustering structures in the ground state of ^{12}Be nucleus through the $(p, p\alpha)$ reaction at 250 MeV. The target and residual nuclei are described by the new framework of a nonlocalized cluster model with valence neutrons, and the reaction process is treated in the DWIA framework. The rich phenomena in the low-lying states of ^{12}Be target, such as the coexistence of binary cluster and MO configurations, are described by the superposition of bases extending the THSR wave functions. The low-lying energy spectrum and the probabilities of strong and weak clustering components in the ground state of ^{12}Be are obtained by the structural calculations using the newly formulated wave function. It is found that the magic number $N = 8$ breaking occurs because of the strong clustering in the ground state of ^{12}Be. The huge difference in the magnitude of TDXs at the zero momentum between the π-orbit and the $\alpha + {}^8$He configurations shows that the TDX is a good measure for the breaking of $N = 8$. In addition, the TDX is found to be highly sensitive to the strong and weak cluster formations, which allows quantitative discussions for the corresponding mixing ratio in the ground state of ^{12}Be. This study provides a feasible approach to probe directly the exotic clustering features in the ground state of ^{12}Be. Furthermore, the new THSR wave function formulated in this work provides new option for the study of neutron-rich nuclei near the drip line.

ACKNOWLEDGMENTS

The authors thank K. Minomo, Y. Neoh, Y. Chazono, and N. Itagaki for valuable discussions. The computation was carried out with the computer facilities at the Research Center for Nuclear Physics, Osaka University. This work was supported in part by Grants-in-Aid of the Japan Society for the Promotion of Science (Grants No. JP16K05352, No. JP15J01392, and No. JP18K03617).

APPENDIX: FORMULATIONS OF CLUSTER AND MOLECULAR ORBIT STATES

We prepare the cluster and the molecular orbit states by the new extension of the THSR formulations used in our previous work [47,48].

1. The α cluster and the ^{8}He cluster

To simplify the discussion, we define the Gaussian wave packet in real space for nucleons as

$$g(\boldsymbol{r}, \boldsymbol{R}) = \left(\frac{1}{\pi b^2}\right)^{3/4} \exp\left\{-\frac{(\boldsymbol{r} - \boldsymbol{R})^2}{2b^2}\right\}, \tag{A1}$$

and the s states of nucleons are written as the product of the spatial wave packet and the spin-isospin term,

$$\phi^s_{\tau s}(\boldsymbol{r}, \boldsymbol{R}) = g(\boldsymbol{r}, \boldsymbol{R})\,|\tau, s\rangle\,. \tag{A2}$$

The α clusters are described by the antisymmetrization of four s states with spin-isospin saturation, as

$$\Psi_\alpha(\boldsymbol{R}) = \frac{1}{\sqrt{4!}}\mathcal{A}\{\phi_1\phi_2\phi_3\phi_4\}, \tag{A3}$$

where

$$\begin{aligned}\phi_1 &= \phi^s_{p\uparrow}(\boldsymbol{r}, \boldsymbol{R}), \quad \phi_2 = \phi^s_{p\downarrow}(\boldsymbol{r}, \boldsymbol{R}),\\ \phi_3 &= \phi^s_{n\uparrow}(\boldsymbol{r}, \boldsymbol{R}), \quad \phi_4 = \phi^s_{n\downarrow}(\boldsymbol{r}, \boldsymbol{R}).\end{aligned} \tag{A4}$$

The ^{8}He-cluster wave function is written as the Slater determinant of eight single-nucleon states, including four s states in α cluster and four surrounding p states, as

$$\begin{aligned}|\Phi(^8\mathrm{He}, \boldsymbol{R})\rangle &= \frac{1}{\sqrt{8!}}\,|\mathcal{A}\{\phi_5\phi_6\phi_7\phi_8\phi_9\phi_{10}\phi_{11}\phi_{12}\}\rangle\\ &= \frac{1}{\sqrt{8!}}\,|\mathcal{A}\{\phi_\alpha(\boldsymbol{R})\phi_9\phi_{10}\phi_{11}\phi_{12}\}\rangle\,,\end{aligned} \tag{A5}$$

where ϕ_5–ϕ_8 denote the s states and ϕ_9–ϕ_{12} denote the p states. The states ϕ_9 and ϕ_{10} correspond to the $1P_{3/2,\pm 3/2}$ states with the ring-type distribution on the horizontal plane, and they are simulated by the integration

$$\begin{aligned}&\phi_{9,10}(\boldsymbol{r}, \boldsymbol{R})\\ &= \int d\boldsymbol{R}'\mathcal{G}(\boldsymbol{R}', \boldsymbol{\beta}_p)e^{\pm i\phi_{\boldsymbol{R}'}}g(\boldsymbol{r}, \boldsymbol{R} + \boldsymbol{R}')\,|\tau, \sigma = \pm 1/2\rangle\,.\end{aligned} \tag{A6}$$

In the limit of $\boldsymbol{\beta}_p \to \mathbf{0}$ fm, the states ϕ_9 and ϕ_{10} converge to the $1P_{3/2,\pm 3/2}$ states of the harmonic oscillators. For the other two p states in the ^{8}He cluster, we project the desired $1P_{3/2,\pm 1/2}$ states from the vertical rotation of states ϕ_9 and ϕ_{10}, as

$$\begin{aligned}\phi_{11}(\boldsymbol{r},\boldsymbol{R}) &= \hat{R}(\Omega)\phi_9(\boldsymbol{r},\boldsymbol{R}),\\ \phi_{12}(\boldsymbol{r},\boldsymbol{R}) &= \hat{R}(\Omega)\phi_{10}(\boldsymbol{r},\boldsymbol{R}),\end{aligned} \tag{A7}$$

where the Euler angle Ω is $\{0, \pi/2, 0\}$. Because of the total antisymmetrization between the four neutron states ϕ_9–ϕ_{12} in the $1P_{3/2}$ orbits, only the $1P_{3/2,\pm 1/2}$ components of the rotated states ϕ_{11} and ϕ_{12} contribute to the total cluster wave function of ^{8}He.

2. The π-orbit states

The π orbits are written as [47]

$$\phi^{\pi}_{\tau s}(\boldsymbol{r}) = \int d\boldsymbol{R}'\mathcal{G}(\boldsymbol{R}',\boldsymbol{\beta}_\pi)e^{\pm i\phi_{\boldsymbol{R}'}}g(\boldsymbol{r}_i,\boldsymbol{R}')\,|\tau, s=\pm 1/2\rangle\,, \tag{A8}$$

and

$$\phi^{\pi*}_{\tau s}(\boldsymbol{r}) = \int d\boldsymbol{R}'\mathcal{G}(\boldsymbol{R}',\boldsymbol{\beta}'_\pi)e^{\pm i\phi_{\boldsymbol{R}'}}g(\boldsymbol{r}_i,\boldsymbol{R}')\,|\tau, s=\mp 1/2\rangle\,, \tag{A9}$$

where the superscripts π and $\pi*$ denote the π orbits with parallel and antiparallel spin-isospin coupling, respectively. The states ϕ^{π}_9–ϕ^{π}_{12} of four neutrons occupying π orbits in Eqs. (7) and (9) are defined as

$$\begin{aligned}\phi^{\pi}_9 &= \phi^{\pi}_{n\uparrow}(\boldsymbol{r}), \quad \phi^{\pi}_{10} = \phi^{\pi}_{n\downarrow}(\boldsymbol{r}),\\ \phi^{\pi*}_{11} &= \phi^{\pi*}_{n\uparrow}(\boldsymbol{r}), \quad \phi^{\pi*}_{12} = \phi^{\pi*}_{n\downarrow}(\boldsymbol{r}).\end{aligned} \tag{A10}$$

3. The σ-orbit states

The σ orbits in the ^{12}Be nucleus are formulated with respect to the α clusters as

$$\phi^{\sigma}_{\tau s}(\boldsymbol{r},\boldsymbol{R}) = \int d\boldsymbol{R}'\mathcal{G}(\boldsymbol{R}',\boldsymbol{\beta}_\sigma)\mathcal{F}(\boldsymbol{R})\mathcal{F}(\boldsymbol{R}')g(\boldsymbol{r},\boldsymbol{R}+\boldsymbol{R}')\,|\tau, s\rangle\,, \tag{A11}$$

TABLE II. Parameters of the THSR basis states in the $\alpha + {}^8$He, π-orbit, and σ-orbit configurations. Detailed explanations of the parameters are given in the main text. All units are in fm.

Basis	$\beta_{\alpha,xy}$	$\beta_{\alpha,z}$	$\beta^{9,10}_{n,xy}$	$\beta^{9,10}_{n,z}$	$\beta^{11,12}_{n,xy}$	$\beta^{11,12}_{n,z}$
$\Phi_{\alpha+{}^8\mathrm{He}}$	0.1	2.0, 3.0, 4.0	0.1	0.4	0.1	0.4
$\Phi_{\pi\text{-orbit}}$	0.1	2.0, 3.0, 4.0	1.5	3.0	2.5	3.0
$\Phi_{\sigma\text{-orbit}}$	0.1	2.0, 3.0, 4.0	1.5	3.0	0.1	2.0

where $\pm\boldsymbol{R}$ are the generate coordinates of two α clusters in Eq. (9). The factor functions $\mathcal{F}$ are defined by

$$\mathcal{F}(\boldsymbol{R}) = \begin{cases}+1 & (R_z > 0)\\ -1 & (R_z < 0).\end{cases} \tag{A12}$$

In Eq. (9), there is integration over the α-cluster generate coordinate $\boldsymbol{R}$, as

$$\begin{aligned}&\int d\boldsymbol{R}\mathcal{G}(\boldsymbol{R},\boldsymbol{\beta})\phi^{\sigma}_{\tau s}(\boldsymbol{r},\boldsymbol{R})\\ &\quad= \int d\boldsymbol{R}d\boldsymbol{R}'\mathcal{G}(\boldsymbol{R},\boldsymbol{\beta})\mathcal{G}(\boldsymbol{R}',\boldsymbol{\beta}_\sigma)\mathcal{F}(\boldsymbol{R})\mathcal{F}(\boldsymbol{R}')\\ &\qquad\times g(\boldsymbol{r},\boldsymbol{R}'+\boldsymbol{R})\,|\tau, s\rangle\,,\end{aligned} \tag{A13}$$

which numerically describes the single-nucleon state in the σ-orbit configuration, as shown by the corresponding density distribution in Fig. 2(b). The states ϕ^{σ}_{11} and ϕ^{σ}_{12} of two neutrons occupying the σ orbits in Eq. (9) are defined as

$$\phi^{\sigma}_{11} = \phi^{\sigma}_{n\uparrow}(\boldsymbol{r},\boldsymbol{R}), \quad \phi^{\sigma}_{12} = \phi^{\sigma}_{n\downarrow}(\boldsymbol{r},\boldsymbol{R}). \tag{A14}$$

4. Parameters of the Tohsaki–Horiuchi–Schuck–Röpke bases

We list in Table II the parameters of the THSR basis states used in the numerical calculation. In the table, β_αs are parameters for the cluster motion in each configuration as shown in Eqs. (6), (7), and (9). For the $\alpha + {}^8$He configuration, β_ns denote parameters β_ps for the neutrons occupying the p orbits in the ^{8}He cluster, as shown in Eqs. (A6) and (A7). For the π-orbit and σ-orbit configurations, β_ns denote parameters β_πs and β_σs, respectively, for neutrons occupying the MO orbits, as shown in Eqs. (A8), (A9), and (A11). The superscripts 9–12 denote parameters for the corresponding single-neutron states ϕ_9–ϕ_{12} in each configuration.

[1] M. Freer, H. Horiuchi, Y. Kanada-En'yo, D. Lee, and Ulf-G. Meißner, Rev. Mod. Phys. **90**, 035004 (2018).
[2] Y. Kanada-En'yo and H. Horiuchi, Prog. Theor. Phys. Suppl. **142**, 205 (2001).
[3] N. Itagaki, S. Okabe, and K. Ikeda, Prog. Theor. Phys. Suppl. **142**, 297 (2001).
[4] W. von Oertzen, M. Freer, and Y. Kanada-En'yo, Phys. Rep. **432**, 43 (2006).
[5] Y. Kanada-En'yo, M. Kimura, and A. Ono, Prog. Theor. Exp. Phys. **2012**, 01A202 (2012).
[6] H. Horiuchi, K. Ikeda, and K. Katō, Prog. Theor. Phys. Suppl. **192**, 1 (2012).
[7] M. Ito and K. Ikeda, Rep. Prog. Phys. **77**, 096301 (2014).
[8] Z. Ren and B. Zhou, Front. Phys. **13**, 132110 (2018).
[9] A. Tohsaki, H. Horiuchi, P. Schuck, and G. Röpke, Phys. Rev. Lett. **87**, 192501 (2001).
[10] S. Okabe, Y. Abe, and H. Tanaka, Prog. Theor. Phys. **57**, 866 (1977).
[11] M. Seya, M. Kohno, and S. Nagata, Prog. Theor. Phys. **65**, 204 (1981).

[12] P. Descouvemont, Phys. Rev. C **39**, 1557 (1989).
[13] W. von Oertzen, Z. Phys. A: Hadrons Nucl. **354**, 37 (1996).
[14] K. Arai, Y. Ogawa, Y. Suzuki, and K. Varga, Phys. Rev. C **54**, 132 (1996).
[15] A. Doté, H. Horiuchi, and Y. Kanada-En'yo, Phys. Rev. C **56**, 1844 (1997).
[16] Y. Kanada-En'yo, H. Horiuchi, and A. Doté, Phys. Rev. C **60**, 064304 (1999).
[17] Y. Ogawa, K. Arai, Y. Suzuki, and K. Varga, Nucl. Phys. A **673**, 122 (2000).
[18] N. Itagaki and S. Okabe, Phys. Rev. C **61**, 044306 (2000).
[19] P. Descouvemont, Nucl. Phys. A **699**, 463 (2002).
[20] M. Ito, K. Kato, and K. Ikeda, Phys. Lett. B **588**, 43 (2004).
[21] M. Ito, N. Itagaki, H. Sakurai, and K. Ikeda, Phys. Rev. Lett. **100**, 182502 (2008).
[22] M. Ito, N. Itagaki, and K. Ikeda, Phys. Rev. C **85**, 014302 (2012).
[23] Y. Kanada-En'yo and H. Horiuchi, Phys. Rev. C **68**, 014319 (2003).
[24] F. Kobayashi and Y. Kanada-En'yo, Phys. Rev. C **86**, 064303 (2012).
[25] Y. Kanada-En'yo, Phys. Rev. C **94**, 024326 (2016).
[26] P. G. Roos, N. S. Chant, A. A. Cowley, D. A. Goldberg, H. D. Holmgren, and R. Woody, III, Phys. Rev. C **15**, 69 (1977).
[27] A. Nadasen, N. S. Chant, P. G. Roos, T. A. Carey, R. Cowen, C. Samanta, and J. Wesick, Phys. Rev. C **22**, 1394 (1980).
[28] T. A. Carey, P. G. Roos, N. S. Chant, A. Nadasen, and H. L. Chen, Phys. Rev. C **29**, 1273 (1984).
[29] C. W. Wang, P. G. Roos, N. S. Chant, G. Ciangaru, F. Khazaie, D. J. Mack, A. Nadasen, S. J. Mills, R. E. Warner, E. Norbeck, F. D. Becchetti, J. W. Janecke, and P. M. Lister, Phys. Rev. C **31**, 1662 (1985).
[30] A. Nadasen, P. G. Roos, N. S. Chant, C. C. Chang, G. Ciangaru, H. F. Breuer, J. Wesick, and E. Norbeck, Phys. Rev. C **40**, 1130 (1989).
[31] J. Mabiala, A. A. Cowley, S. V. Förtsch, E. Z. Buthelezi, R. Neveling, F. D. Smit, G. F. Steyn, and J. J. Van Zyl, Phys. Rev. C **79**, 054612 (2009).
[32] K. Yoshida, K. Minomo, and K. Ogata, Phys. Rev. C **94**, 044604 (2016).
[33] T. Wakasa, K. Ogata, and T. Noro, Prog. Part. Nucl. Phys. **96**, 32 (2017).
[34] M. Lyu, K. Yoshida, Y. Kanada-En'yo, and K. Ogata, Phys. Rev. C **97**, 044612 (2018).
[35] K. Yoshida, K. Ogata, and Y. Kanada-En'yo, Phys. Rev. C **98**, 024614 (2018).
[36] F. D. Becchetti, J. Jänecke, and C. E. Thorn, Nucl. Phys. A **305**, 313 (1978).
[37] N. Anantaraman, H. E. Gove, R. A. Lindgren, J. Tōke, J. P. Trentelman, J. P. Draayer, F. C. Jundt, and G. Guillaume, Nucl. Phys. A **313**, 445 (1979).
[38] T. Tanabe, M. Yasue, K. Sato, K. Ogino, Y. Kadota, Y. Taniguchi, K. Obori, K. Makino, and M. Tochi, Phys. Rev. C **24**, 2556 (1981).
[39] T. Fukui, Y. Taniguchi, T. Suhara, Y. Kanada-En'yo, and K. Ogata, Phys. Rev. C **93**, 034606 (2016).
[40] Z. Yang (private communication).
[41] Y. Funaki, H. Horiuchi, and A. Tohsaki, Prog. Part. Nucl. Phys. **82**, 78 (2015).
[42] Y. Funaki, Phys. Rev. C **92**, 021302(R) (2015).
[43] Y. Funaki, Phys. Rev. C **94**, 024344 (2016).
[44] B. Zhou, Y. Funaki, H. Horiuchi, Z. Ren, G. Röpke, P. Schuck, A. Tohsaki, C. Xu, and T. Yamada, Phys. Rev. Lett. **110**, 262501 (2013).
[45] B. Zhou, Y. Funaki, H. Horiuchi, Z. Ren, G. Röpke, P. Schuck, A. Tohsaki, C. Xu, and T. Yamada, Phys. Rev. C **89**, 034319 (2014).
[46] B. Zhou, A. Tohsaki, H. Horiuchi, and Z. Ren, Phys. Rev. C **94**, 044319 (2016).
[47] M. Lyu, Z. Ren, B. Zhou, Y. Funaki, H. Horiuchi, G. Röpke, P. Schuck, A. Tohsaki, C. Xu, and T. Yamada, Phys. Rev. C **91**, 014313 (2015).
[48] M. Lyu, Z. Ren, B. Zhou, Y. Funaki, H. Horiuchi, G. Röpke, P. Schuck, A. Tohsaki, C. Xu, and T. Yamada, Phys. Rev. C **93**, 054308 (2016).
[49] Q. Zhao, Z. Ren, M. Lyu, H. Horiuchi, Y. Funaki, G. Röpke, P. Schuck, A. Tohsaki, C. Xu, T. Yamada, and B. Zhou, Phys. Rev. C **97**, 054323 (2018).
[50] K. Amos, P. J. Dortmans, H. V. von Geramb, S. Karataglidis, and J. Raynal, in *Advances in Nuclear Physics*, edited by J. W. Negele and E. Vogt (Plenum, New York, 2000), Vol. 25, p. 275.
[51] P. Ring and P. Schuck, in *The Nuclear Many-Body Problem* (Springer-Verlag, New York, 1980), p. 473.
[52] D. M. Brink, in *International School of Physics "Enrico Fermi," XXXVI*, edited by C. Bloch (Academic Press, New York, 1966), p. 247.
[53] Y. Kanada-En'yo, T. Suhara, and Y. Taniguchi, Prog. Theor. Exp. Phys. **2014**, 073D02 (2014).
[54] C. A. Bertulani, Phys. Rev. Lett. **94**, 072701 (2005).
[55] K. Ogata and C. A. Bertulani, Prog. Theor. Phys. **121**, 1399 (2009).
[56] K. Ogata and C. A. Bertulani, Prog. Theor. Phys. **123**, 701 (2010).
[57] W. H. Long and C. A. Bertulani, Phys. Rev. C **83**, 024907 (2011).
[58] T. Ando, K. Ikeda, and A. Tohsaki-Suzuki, Prog. Theor. Phys. **64**, 1608 (1980).
[59] N. Yamaguchi, T. Kasahara, S. Nagata, and Y. Akaishi, Prog. Theor. Phys. **62**, 1018 (1979).
[60] Y. Kanada-En'yo and H. Horiuchi, Phys. Rev. C **66**, 024305 (2002).
[61] T. Aumann, C. A. Bertulani, and J. Ryckebusch, Phys. Rev. C **88**, 064610 (2013).
[62] L. Atar *et al.* (R^3B Collaboration), Phys. Rev. Lett. **120**, 052501 (2018).
[63] H. N. Liu *et al.*, Phys. Rev. Lett. **122**, 072502 (2019).